




RESEARCH PAPER



Distinct roles of core autophagy-related genes in zebrafish definitive hematopoiesis

Xiang-Ke Chen ^{a,b}, Zhen-Ni Yi ^a, Jack Jark-Yin Lau^a, and Alvin Chun-Hang Ma ^a

^aDepartment of Health Technology and Informatics, The Hong Kong Polytechnic University, Hong Kong, China; ^bDivision of Life Science, The Hong Kong University of Science and Technology, Hong Kong, China

ABSTRACT

Despite the well-described discrepancy between ATG (macroautophagy/autophagy-related) genes in the regulation of hematopoiesis, varying essentiality of core ATG proteins in vertebrate definitive hematopoiesis remains largely unclear. Here, we employed zebrafish (*Danio rerio*) to compare the functions of six core *atg* genes, including *atg13*, *becn1* (beclin1), *atg9a*, *atg2a*, *atg5*, and *atg3*, in vertebrate definitive hematopoiesis via clustered regularly interspaced short palindromic repeats (CRISPR)-Cas9 ribonucleoprotein and morpholino targeting. Zebrafish with various *atg* mutations showed autophagic deficiency and presented partially consistent hematopoietic abnormalities during early development. All six *atg* mutations led to a declined number of *spi1b*⁺ (Spi-1 proto-oncogene b) myeloid progenitor cells. However, only *becn1* mutation resulted in the expansion of *myb*⁺ (v-myb avian myeloblastosis viral oncogene homolog) hematopoietic stem and progenitor cells (HSPCs) and transiently increased *coro1a*⁺ (coronin, actin binding protein, 1A) leukocytes, whereas *atg3* mutation decreased the number of HSPCs and leukocytes. Proteomic analysis of caudal hematopoietic tissue identified *sin3aa* (SIN3 transcription regulator family member Aa) as a potential modulator of *atg13*- and *becn1*-regulated definitive hematopoiesis. Disruption of *sin3aa* rescued the expansion of HSPCs and leukocytes in *becn1* mutants and exacerbated the decrease of HSPCs in *atg13* mutants. Double mutations were also performed to examine alternative functions of various *atg* genes in definitive hematopoiesis. Notably, *becn1* mutation failed to induce HSPCs expansion with one of the other five *atg* mutations. These findings demonstrated the distinct roles of *atg* genes and their interplays in zebrafish definitive hematopoiesis, thereby suggesting that the vertebrate definitive hematopoiesis is regulated in an *atg* gene-dependent manner.

Abbreviations: AGM: aorta-gonad-mesonephros; AO: acridine orange; *atg*: autophagy related; *becn1*: beclin 1, autophagy related; CHT: caudal hematopoietic tissue; CKO: conditional knockout; *coro1a*: coronin, actin binding protein, 1A; CQ: chloroquine; CRISPR: clustered regularly interspaced short palindromic repeats; dpf: days post fertilization; FACS: fluorescence-activated cell sorting; *hbae1.1*: hemoglobin, alpha embryonic 1.1; HSCs: hematopoietic stem cells; HSPCs: hematopoietic stem and progenitor cells; KD: knockdown; KO: knockout; *map1lc3/lc3*: microtubule-associated protein 1 light chain 3; MO: morpholino; *mpeg1.1*: macrophage expressed 1, tandem duplicate 1; *mpx*: myeloid-specific peroxidase; *myb*: v-myb avian myeloblastosis viral oncogene homolog; PE: phosphatidylethanolamine; *p-H3*: phospho-H3 histone; PtdIns3K: class 3 phosphatidylinositol 3-kinase; *rag1*: recombination activating 1; *rb1cc1/fip200*: RB1-inducible coiled-coil 1; RFLP: restriction fragment length polymorphism; RNP: ribonucleoprotein; *sin3aa*: SIN3 transcription regulator family member Aa; *spi1b*: Spi-1 proto-oncogene b; *ulk*: unc-51 like autophagy activating kinase; *vtg1*: vitellogenin 1; WISH: whole-mount in situ hybridization.

ARTICLE HISTORY

Received 11 November 2021
Revised 3 October 2023
Accepted 17 October 2023



KEYWORDS


Autophagy-related genes; CRISPR-Cas9 ribonucleoprotein; definitive hematopoiesis; hematopoietic stem and progenitor cells; zebrafish

Introduction

Macroautophagy (hereinafter autophagy) serves as the scavenger of the cells by removal of harmful components via the lysosomal degradation, which, as an essential but complex process, is tightly regulated by a category of genes, namely ATG (autophagy-related) genes [1]. Approximately 20 core ATG proteins that orchestrate the critical steps of canonical autophagy were classified into six functional groups/machineries, including the ULK1 (unc-51 like autophagy activating kinase 1) complex (initiation), the class 3 phosphatidylinositol 3-kinase (PtdIns3K) complex (phagophore membrane nucleation), ATG9A-containing vesicles

(providing membrane), ATG2A complex (membrane expansion), ATG12 conjugation system (membrane expansion and linking MAP1LC3/LC3 [microtubule associated protein 1 light chain 3] with phosphatidylethanolamine [PE]), and LC3–PE conjugation system (membrane expansion and target recognition), which are highly conserved across the eukaryotes [2]. Loss of core *Atg* genes commonly results in neonatal lethality in mice, while the exact cause of death remains elusive [3]. Despite the well-known essentiality of core *Atg* genes in mice, a recent clinical study reported the identification of twelve patients from five families who survived with severely impaired autophagy

CONTACT Alvin Chun-Hang Ma  alvin.ma@polyu.edu.hk  Department of Health Technology and Informatics, The Hong Kong Polytechnic University, Rm. Y928, Lee Shau Kee Building, Hong Kong, China

 Supplemental data for this article can be accessed online at <https://doi.org/10.1080/15548627.2023.2274251>

© 2023 Informa UK Limited, trading as Taylor & Francis Group

due to the loss of *ATG7*, one of the most well-studied core *ATG* genes [4]. This was ascribed to the non-canonical or alternative autophagy that undergoes in the absence of some core *ATG* genes because the autophagosomes could still be formed [4,5]. Many autophagic pathways independent of core *Atg* genes, such as those that bypass *Ulk1*, *Becn1*, *Atg5* or *Atg7*, as well as the autophagy-independent functions of core *Atg* genes have also been identified in mice over the past decade [6,7]. Nevertheless, the majority of previous studies still focused on canonical autophagy, and the distinctive effects of various core *ATG* genes are largely neglected.

Previous studies have shown the resemblance and discrepancy between core *Atg* genes in the regulation of mouse hematopoiesis, which is a vital biological process of blood cellular component formation, although very few of them included more than one *Atg* gene [8]. In definitive hematopoiesis, *atg5*, *atg7*, or *rb1cc1/fip200* (RB1-inducible coiled-coil 1) conditional knockout (CKO) in hematopoietic cells declined the number of hematopoietic stem cells (HSCs) [9–11], whereas *becn1* or *atg12* CKO failed to alter the total number of HSCs [12,13]. Moreover, *atg5* or *atg7* CKO reduced the number of multi-lineage progenitor cells [9,10]; in contrast, their number increased and remained unchanged in *atg12* and *becn1* CKO, respectively [12,13]. Among *atg5*, *becn1*, *atg7*, *atg12*, and *rb1cc1* CKOs, myeloproliferation was only observed in *atg7*, *atg12* or *rb1cc1* CKO mice, while anemia was found in *atg5*, *atg7*, or *rb1cc1* CKO mice [9–13]. These differential hematopoietic abnormalities found in CKO of the core *Atg* genes demonstrated the *Atg* genes-dependency of hematopoiesis, while more studies on other core *Atg* genes are needed. In addition to the differences between *Atg* genes, contradictory results in the regulation of hematopoiesis were also observed in CKOs of core *Atg* genes, including *Atg5* and *Atg7* [9,13,14]. Besides, *Atg7* was found to be indispensable for adult but not for neonatal HSCs in mice [14], which suggested the important “timing” of various core *Atg* genes in the regulation of hematopoiesis. However, whether this “timing” also occurs in other core *Atg* genes or not remains unexplored.

Over the past decades, zebrafish (*Danio rerio*), a tropical freshwater fish, has emerged as a vital genetic model in the research field of hematopoiesis as well as autophagy due to its genetic tractability, small and transparent body, *in vitro* embryogenesis, and, more importantly, evolutionarily conserved genes orthologous to around 70% of the human genes [15–17]. With advanced gene editing tools, such as morpholino (MO) [18], transcription activator-like effector nucleases (TALEN) [19], and clustered regularly interspaced short palindromic repeats (CRISPR)-Cas9 [20], zebrafish embryos have gradually become a more efficient, convenient, and feasible model than mice in genetic screening *in vivo*, particularly in the studies of hematopoiesis. Nevertheless, the roles of core *atg* genes in zebrafish hematopoiesis remain largely unknown. Here, we reported for the first time, the differential effects of *atg* mutations via CRISPR-Cas9 ribonucleoprotein (RNP) or MO targeting on zebrafish definitive hematopoiesis, although their mutations all disturbed the autophagy process, which highlighted the essentiality of

various *atg* gene-dependent effects rather than the uniformed canonical autophagy-dependent effect on vertebrate definitive hematopoiesis.

Results

Core *atg* gene targeting by CRISPR-Cas9 ribonucleoprotein

Core *ATG* genes that are required for the autophagy process have been classified into six evolutionarily conserved functional groups, also known as “core autophagy machineries” [2]. In this study, core *atg* genes were selected from the six core machineries of autophagy for CRISPR-Cas9 RNP targeting, including *atg13* (ULK1 complex), *becn1* (PtdIns3K complex), *atg9a* (ATG9A-containing vesicles), *atg2a* (ATG2A complex), *atg5* (ATG12 conjugation system), and *atg3* (LC3-PE conjugation system) (Figure 1A–B). Phylogenetic analysis revealed that these *atg* genes were conserved between zebrafish and humans with high similarities (Figure S1A–D). Single guide RNA (sgRNA) was designed for each *atg* gene targeting early exon to model null-like mutation in zebrafish embryos (Figure 1C). Very high mutagenesis efficiencies (>95%) were obtained in all somatic *atg* mutants as shown by restriction fragment length polymorphism (RFLP) assay (Figure 1D) and Sanger sequencing (Figure S1E), which can result in null-like loss of *Atg* protein (Figure S2A). In addition, stable production of null-like zebrafish mutants can be achieved by the skilled operator (Figure S2B). While most of the mutant embryos (>75%) displayed normal development and morphology in embryonic stages (Figure 1E), a small proportion of them were deformed in all the *atg* mutants (Figure S2C). Most of these mutants can only survive up to around 2 weeks post-fertilization, except *atg9a* and *atg2a* mutants who can survive to adulthood. In addition, MOs targeting six *atg* genes were used in parallel (Figure 1F), which also resulted in normal development and morphology in the majority of zebrafish mutants (Figure 1G) and similar deformed phenotypes (Figure S2D).

Autophagy deficiency in core *atg* mutant zebrafish embryos

We next examined autophagy levels after *atg* genes targeting in *Tg(GFP-Lc3)* zebrafish line. The number of *Lc3*⁺ autophagy puncta (autophagosome) in the muscle was significantly lowered in *atg13*, *becn1*, *atg9a*, *atg5*, and *atg3* mutants but not in *atg2a* mutants (Figure 2A–C). The inconsistent autophagic activation or basal level was not only detected among different *atg* mutations but also among various organs and tissues (Figure S2G). Intriguingly, none of the *atg* mutations can completely block autophagy, which suggests the presence of individual *atg* gene-independent alternative autophagy. A consistent autophagic defect was also observed in different tissues of zebrafish embryos with MO-dependent *atg* gene knockdown (KD) (Figure 2D–F). In addition, autophagy flux was measured upon chloroquine (CQ) treatment or using *Tg(GFP-Lc3:RFP-Lc3ΔG)* zebrafish line. An elevated number of puncta was observed in the control (CTRL), *becn1*, *atg9a*, and

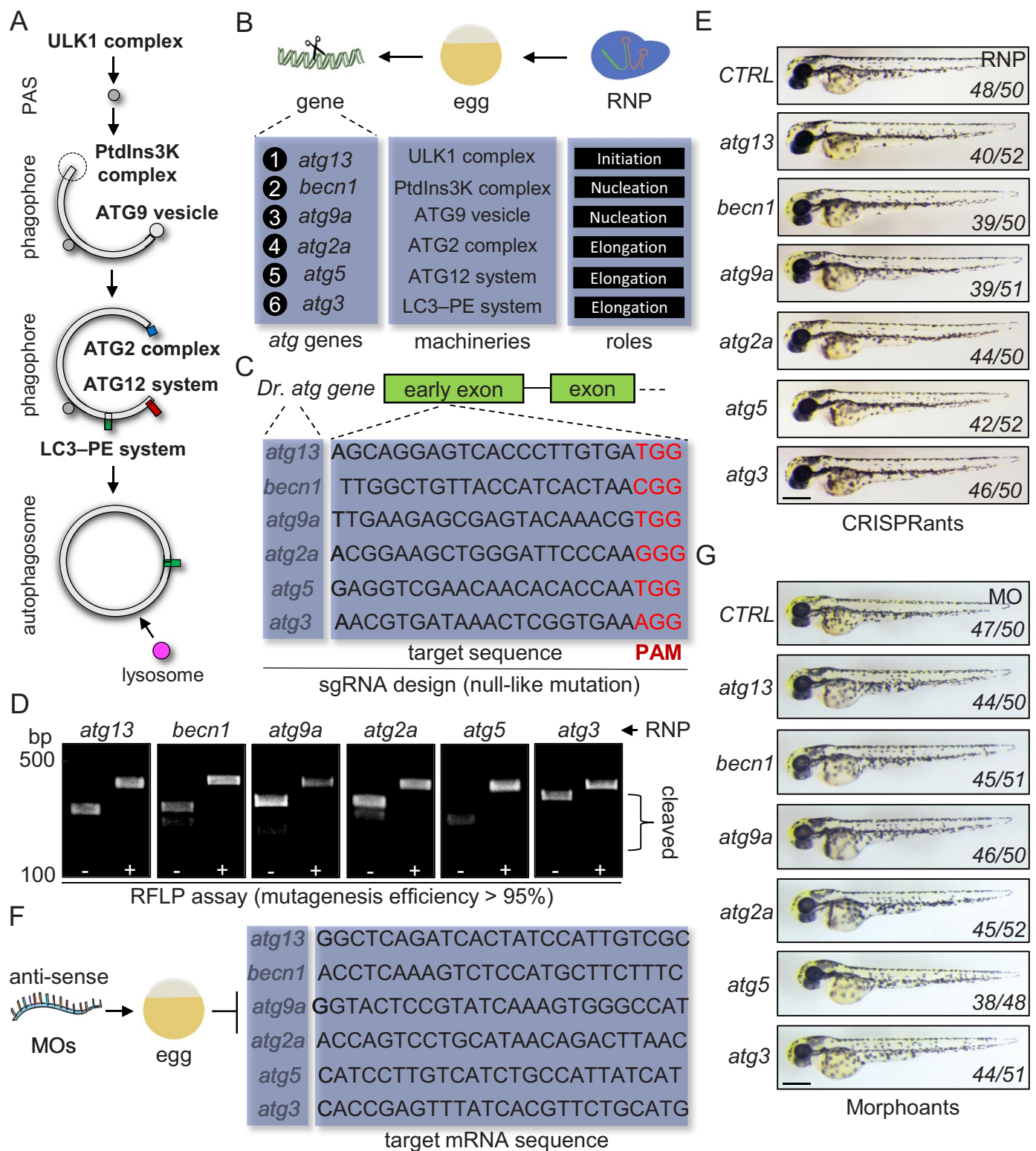


Figure 1. Core *atg* genes targeting by CRISPR-Cas9 ribonucleoprotein and morpholino. (A) schematic diagram showing the involvement of autophagy machineries in the autophagy pathway. PAS, pre-autophagosomal structure. (B) schematic diagram showing the CRISPR-Cas9 ribonucleoprotein (RNP) targeting and core *atg* (autophagy-related) genes selected from autophagy machineries. (C) target sequences and sgRNA design for various *atg* genes in zebrafish. (D) restriction fragment length polymorphism (RFLP) assay and mutation efficiency of various *atg* genes-targeting sgRNAs. (E) representative morphology of 2 days post-fertilization (dpf) zebrafish embryos with *atg* mutations. Scale bar: 0.5 mm. (F) target sequences and morpholino (MO) design for various *atg* genes in zebrafish. (G) representative morphology of 2 dpf zebrafish embryos injected with MO targeting *atg* genes. Scale bar: 0.5 mm.

atg5 mutants after CQ treatment, while it remained unchanged in *atg13*, *atg2a*, and *atg3* mutants (Figure 2A–C). Similarly, an increased ratio of *GFP-Lc3:RFP-Lc3ΔG* was

observed in both CRISPR-Cas9 RNP- and MO-based *atg13* and *atg2a* mutant zebrafish embryos (Figure 2G–K), suggesting impaired autophagic flux in *atg13* and *atg2a* mutants.

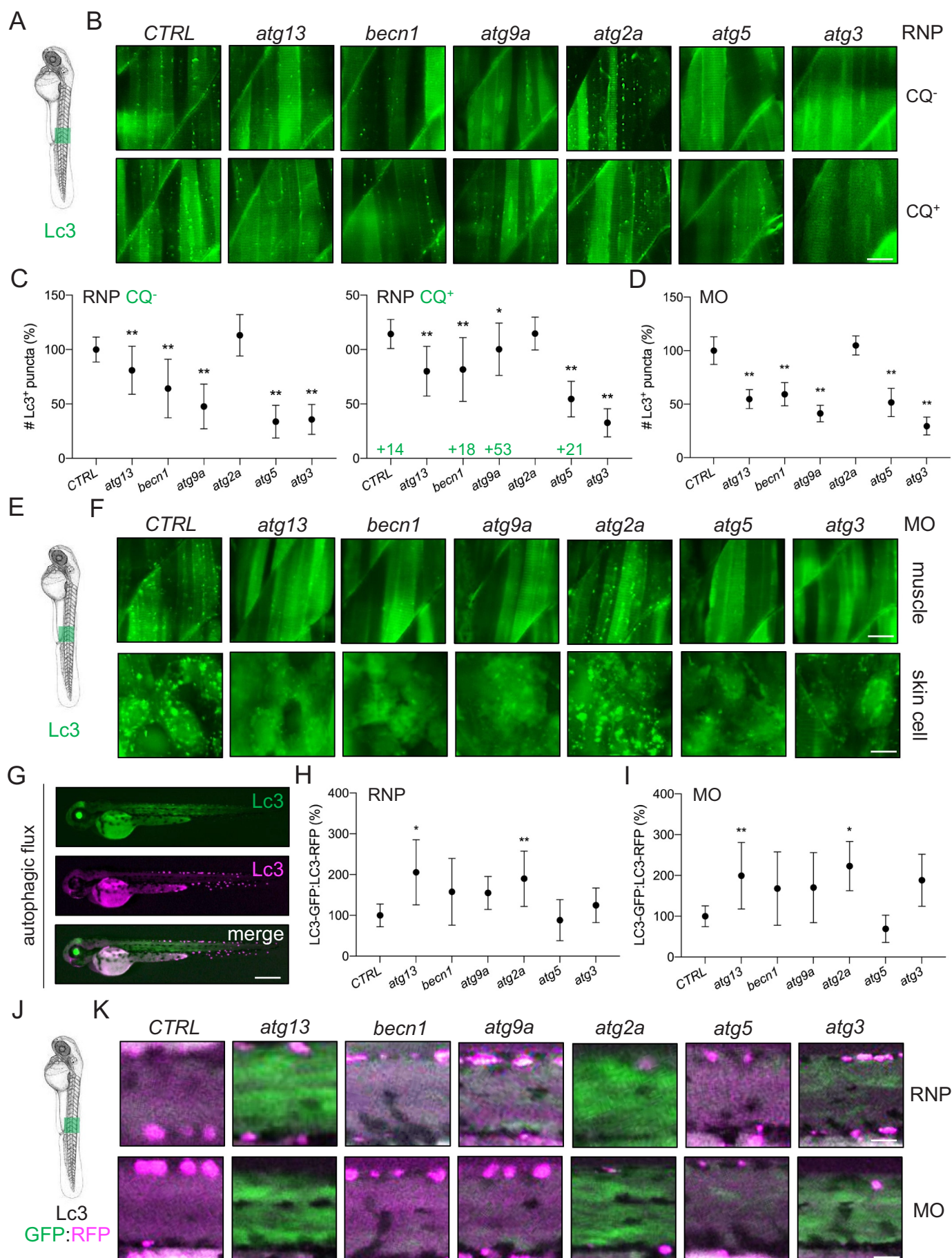


Figure 2. Autophagic deficiency in zebrafish embryos with core *atg* mutations. (A-B) autophagosomes or Lc3⁺ puncta in the muscle of various *atg* mutant *Tg(GFP-Lc3)* zebrafish embryos with (+) and without (-) chloroquine (CQ) treatment at 2 dpf. Scale bar: 50 μ m. (C-D) autophagosomes or Lc3⁺ puncta in the muscle and skin cells

Consistent with the observed autophagic changes in muscle cells, the western blot of whole embryos showed a similar reduction in the Lc3-II levels in various *atg* mutants other than *atg13*, which also indicated the tissue-specific autophagic changes (Figure S2E,F). More importantly, a more sensitive Cyto-ID autophagy staining [21] was performed in the sorted *coro1a*⁺ (coronin, actin binding protein, 1A) hematopoietic cells via fluorescence-activated cell sorting (FACS) since very few *Lc3*⁺ puncta can be detected in the *coro1a*⁺ cells of *Tg* (*GFP-Lc3;coro1a:DsRed*) zebrafish line (Figure S2H) and Cyto-ID autophagy dye failed to penetrate the live zebrafish embryo. Importantly, Cyto-ID⁺ autophagic vacuoles declined in almost all *atg* mutants similar to the decreased number of puncta in the muscle (Figure 3A–C), demonstrating that *atg* mutations resulted in autophagy deficiency in the hematopoietic cells.

Distinct effects of *atg* mutations on zebrafish definitive hematopoiesis

We then examined the effects of *atg* mutations on definitive hematopoiesis by whole-mount *in situ* hybridization (WISH). Although all the *atg* mutations resulted in autophagy deficiency, only *becn1* mutation caused *myb*⁺ (v-myb avian myeloblastosis viral oncogene homolog) hematopoietic stem and progenitor cells (HSPCs) expansion in aortagonad-mesonephros (AGM) and caudal hematopoietic tissue (CHT) in zebrafish embryos at 30 and 48 h post-fertilization (hpf), respectively (Figure 4A–F). In contrast, *atg13* and *atg3* mutations decreased the number of *myb*⁺ HSPCs in the CHT at 48 hpf, albeit modestly (<30%), and *atg9a*, *atg2a*, and *atg5* mutations showed no effects on the number of HSPCs (Figure 4D–F). Alterations in the number of *lcp1*⁺ (lymphocyte cytosolic protein 1) leukocytes were consistent with the change of HSPCs in *becn1*, *atg9a*, *atg2a*, *atg5* ($p = 0.08$), and *atg3* mutant zebrafish embryos, while an opposite change of leukocytes to HSPCs was found in *atg13* mutants (Figure 4J–L). Conversely, *spi1b*⁺ (Spi-1 proto-oncogene b) myeloid progenitor cells consistently declined in all the *atg* mutants (Figure 4G–I), and no significant difference was observed in the *hbae1.1*⁺ (hemoglobin, alpha embryonic 1.1) erythrocytes (Figure 4M–O) and *rag1*⁺ (recombination activating 1) lymphocytes in CHT at 48 hpf and thymus at 96 hpf, respectively (Figure S2I,J). Further, time-dependent effects of *atg* mutations on definitive hematopoiesis were assessed in CRISPR-Cas9 RNP- or MO-based *atg* mutant *Tg*(*myb:GFP*), *Tg*(*spi1b:GFP*), *Tg*(*coro1a:DsRed*), *Tg*(*mpx* [*myeloid-specific peroxidase*]:*GFP*), and *Tg*(*mpeg1.1* [*macrophage expressed 1, tandem duplicate 1*]:*GFP*) (Figure 5A and Figure S3A,B). In consistent with WISH results, *becn1* mutation increased while *atg3* mutation decreased the number of *myb*⁺ HSPCs and *coro1a*⁺ leukocytes in zebrafish embryos from

2 to 4 days post-fertilization(dpf) (Figure 5B–G). Besides, a lower number of *spi1b*⁺ myeloid progenitor cells was found in all the *atg* mutations from 2 to 4 dpf (Figure 5D–E). However, increased *myb*⁺ HSPCs and *coro1a*⁺ leukocytes in *atg13* mutants and increased *coro1a*⁺ leukocytes in *becn1* mutants are transient (Figure 5B–G). Notably, a lowering effect of *atg9a*, *atg2a*, and *atg5* mutations on the number of *myb*⁺ HSPCs was observed in late stages, whereas *atg3* mutation decreased the HSPCs from 2 to 4 dpf (Figure 5B,C). Regarding different myeloid lineages, the change of *mpx*⁺ neutrophils in *atg* mutant zebrafish is consistent with *coro1a*⁺ leukocytes (Figure S4A–C and S5A,B). However, the number of *mpeg1.1*⁺ macrophages was lowered in *atg13*, *becn1*, *atg5*, and *atg3* mutants (Figure S4D,E and S5A,B).

Proteomic analysis of caudal hematopoietic tissue with *atg* mutations

To elucidate the differential effects of *atg* mutation on definitive hematopoiesis, mass spectrometry-based proteomic analysis was performed by using the CHT region of zebrafish embryos to identify the proteomic differences underlying these inconsistent hematopoietic phenotypes (Figure 6A,B). Strikingly, significantly changed proteins identified in mass spectrometry ($p < 0.05$, fold change > 1.50 or < 0.66) varied between *atg* mutations, in which *atg2a* mutation has the lowest number of altered proteins compared with other *atg* genes (Figure 6C). We further examined the similarity of proteomic profiles between different *atg* mutants and found a relatively high number of consistent proteins when comparing *atg5* with *atg13* or *atg3* (Figure 6D). Biological processes enrichment suggested that proteins are primarily involved in nutrition or energy-related processes, such as transport process, metabolic processes, and biogenesis (Figure 6E and Table S2). Of these processes, *atg3* and *becn1* mutations had the highest number of altered proteins in transport and metabolic processes, respectively. More specifically, we identified Sin3aa (SIN3 transcription regulator family member Aa), a crucial epigenetic modifier inconsistently expressed among six *atg* mutations, in which its levels significantly decreased in *atg13* but increased in *becn1* mutants compared to CTRL (Figure 6B, F). Conversely, the protein level of Vtg1 (Vitellogenin 1), an estrogen responder, elevated in all *atg* mutants (Figure 6G). In addition to the distinct proteomic profile, cell death and proliferation were also assessed by using Acridine Orange (AO) and *p-H3* (phospho-histone H3) staining, respectively (Figure 6H,I). The number of AO⁺ and *coro1a*⁺ apoptotic leukocytes increased in *atg13*, *becn1*, and *atg5* mutants, while it remained unchanged in the other *atg* mutants. Besides, *p-H3*⁺ cells undergoing mitosis in the CHT also increased in *becn1* but decreased in *atg5* mutants.

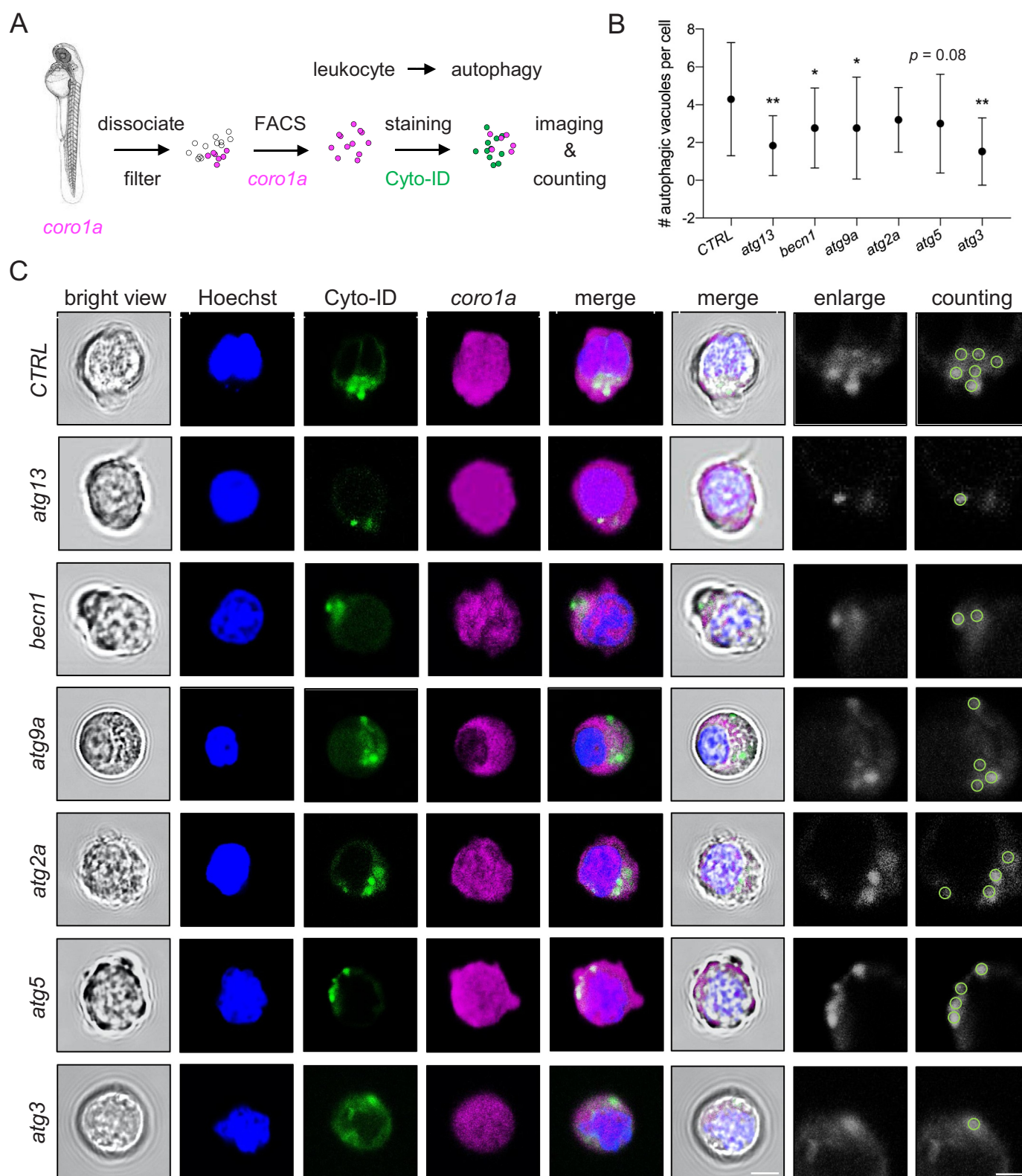


Figure 3. Attenuation of autophagic vacuoles in leukocytes with core *atg* mutations. (A) experimental setup for Cyto-ID⁺ autophagic vacuole measurement in *coro1a*⁺ leukocytes sorted from 2 dpf zebrafish embryos through fluorescence-activated cell sorting (FACS). (B-C) representative images and quantification of Cyto-ID⁺ autophagic vacuoles in *coro1a*⁺ leukocytes sorted from zebrafish embryos with various *atg* mutations. *, $p < 0.05$, **, $p < 0.01$ compared with CTRL, one-way ANOVA with post-hoc Tukey HSD test. Scale bar: 5 μ m.

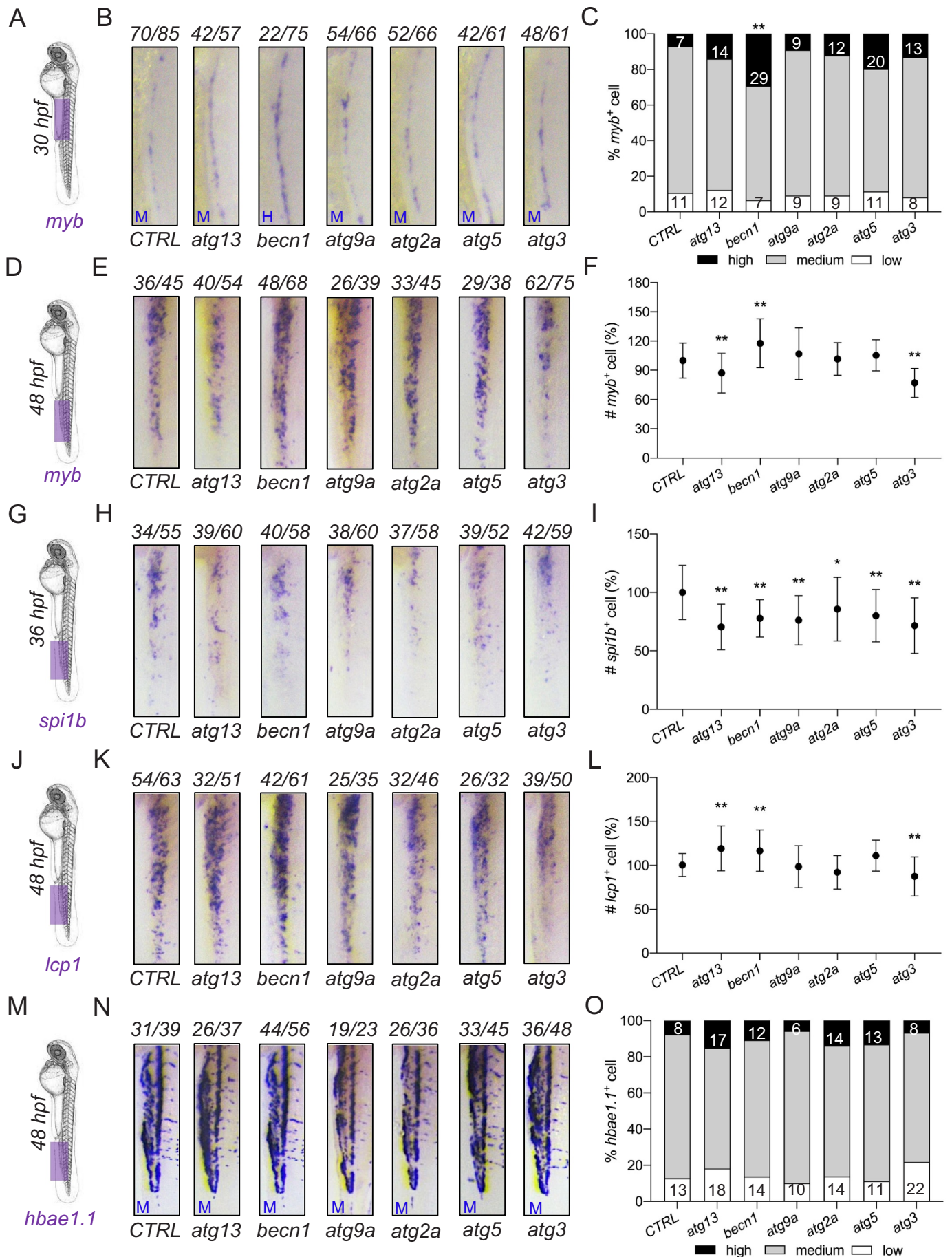


Figure 4. Distinct effects of core *atg* mutations on zebrafish definitive hematopoiesis. (A-C) whole-mount *in situ* hybridization (WISH) results of *myb*⁺ HSPCs in aorta-gonad-mesonephros (AGM) of 30 h post-fertilization (hpf) zebrafish embryos. **, $p < 0.01$ compared with CTRL, chi-squared test. H, high

Involvement of *sin3aa* in core *atg* genes-dependent regulation of HSPCs

We next explored whether *Sin3aa* contributed to the discrepancy in definitive hematopoiesis among *atg* mutations, especially the difference in HSPCs between *atg13* and *becn1* mutants. CRISPR-Cas9 RNP was designed to target *sin3aa* in zebrafish embryos (Figure 7A), which led to a high mutagenesis efficacy but showed no effects on the development and morphology of zebrafish embryos in early stages (Figure 7B,C and Figure S4F). Besides, *sin3aa* mutation alone showed no effects on the definitive hematopoiesis, including *myb*⁺ HSPCs, *spi1b*⁺ myeloid progenitor cells, *coro1a*⁺ leukocytes, *mpx*⁺ neutrophils, and *mpeg1.1*⁺ macrophages, in zebrafish embryos from 2 to 4 dpf (Figure S4G). Notably, co-mutation of *sin3aa* and *becn1* rescued *myb*⁺ HSPCs expansion and transiently increased *coro1a*⁺ leukocytes and *mpx*⁺ neutrophils in CHT from 2 dpf to 4 dpf, while it did not alter the number of *spi1b*⁺ myeloid progenitor cells and *mpeg1.1*⁺ macrophages in *becn1* mutants (Figure 7D–H and Figure S6A). In contrast, *sin3aa* co-mutation exacerbated the lowered number of *myb*⁺ HSPCs in *atg13* mutants, which remained significantly lower than controls at 3 and 4 dpf, and decreased the transiently increased *coro1a*⁺ leukocytes and *mpx*⁺ neutrophils (Figure 7D–G). Similarly, *sin3aa* co-mutation did not affect *spi1b*⁺ myeloid progenitor cells and *mpeg1.1*⁺ macrophages in *atg13* mutants (Figure 7E,H).

Effect of double *atg* mutations on definitive hematopoiesis and autophagy

To further delineate the interplays among *atg* mutations in definitive hematopoiesis, we double-mutated every two core *atg* genes in zebrafish embryos (Figure 8A). High mutagenic efficiencies similar to single CRISPR-Cas9 RNP injection were obtained (Figure S7A). Unlike single *atg* mutation, double mutation resulted in a higher death and deform rate in zebrafish embryos (Figure S7B). Since *atg* genes had been found to be activated rhythmically in a clock-dependent manner, featuring the dynamic mRNA levels of *atg* genes during the early days after birth [22], we also tracked the effect of *atg* double mutations on definitive hematopoiesis including *myb*⁺ HSPCs and *coro1a*⁺ leukocytes from 2 to 4 dpf to examine their potential time-dependent effects. Notably, *myb*⁺ HSPCs and transient *coro1a*⁺ leukocyte expansion in *becn1* mutation can only be found in double mutation with *atg5*, while the other *atg* mutations alleviated the *becn1* mutation-dependent phenotypes (Figure 8B,C and Figure S8A,B). Conversely, a declined number of *myb*⁺ HSPCs in *atg3* mutation was largely independent of the other *atg* mutations, while the decreased number of *coro1a*⁺ leukocytes returned to normal levels after co-mutations with other *atg* mutations (Figure 8B,C). More interestingly, a lower number of *myb*⁺ HSPCs was found in

atg13 mutation when double-mutating with any other *atg* genes except for *becn1* (Figure 8B,C). These synergistic effects of *atg* double mutations in definitive hematopoiesis could be potentially attributed to autophagic alterations and their mutual regulations. The formation of *Lc3*⁺ puncta was robustly blocked in most of the double *atg* mutations in addition to the double-mutation of *atg2a* with *becn1*, *atg9a*, or *atg3* (Figure 8D and Figure S7C). We also evaluated the mRNA levels of six *atg* genes under one of the *atg* mutations, revealing that a single *atg* mutation lowered the mRNA levels of at least some of the other *atg* genes (Figure S7D). Altogether, these results indicate that interplays among core *atg* genes orchestrate the regulation of definitive hematopoiesis in zebrafish embryos.

Discussion

Defective canonical autophagy has long been involved in the hematopoietic disturbances observed in core *Atg* gene-deficient mice [23]. The evidence emerging in the past decade, however, reported the distinct effects of various core *Atg* genes ablation on definitive hematopoiesis [9–13]. It suggested canonical autophagy-independent roles of various core *ATG* genes, largely comprising core *ATG* genes-dependent non-canonical autophagy and non-autophagy functions, in the hematopoietic system, although their roles have been rarely compared. In this context, we hypothesized that the core *ATG* gene has both shared and distinctive functions in definitive hematopoiesis when compared with other core *ATG* genes. Thus, we selected six core *atg* genes from different core autophagy machineries, including *atg13* (ULK1 complex), *becn1* (PtdIns3K complex), *atg9a* (ATG9A-containing vesicles), *atg2a* (ATG2A complex), *atg5* (ATG12 conjugation system), and *atg3* (LC3–PE conjugation system) [2], and examined their functions in zebrafish definitive hematopoiesis using CRISPR-Cas9 RNP and MO targeting. We first observed the autophagy deficiency in the body and hematopoietic cells of various *atg* mutant zebrafish embryos. However, core *atg* mutations showed distinct effects on the definitive hematopoiesis in zebrafish embryos, with some of the effects being time- or cell type-dependent. Further, the mechanisms underlying the discrepancy among various *atg* mutations in definitive hematopoiesis were determined by using proteomic analysis and double mutations. These findings suggested the distinctive roles of core *atg* genes and their interplays in zebrafish definitive hematopoiesis.

Approximately 20 core *ATG* genes that are fundamental to canonical autophagy have been functionally categorized into six core autophagy machineries [2]. Since canonical autophagy is essential for development, mutations of core *atg* genes corresponding to various core autophagy machineries except for *atg9a* and *atg2a* in the present study resulted in larval

group; M, medium group. (D–F) WISH results of *myb*⁺ HSPCs in caudal hematopoietic tissue (CHT) of 48 hpf zebrafish embryos. **, $p < 0.01$ compared with CTRL, one-way ANOVA with post-hoc Tukey HSD test. (G–I) WISH results of *spi1b*⁺ myeloid progenitor cells in CHT of 36 hpf zebrafish embryos. *, $p < 0.05$, **, $p < 0.01$ compared with CTRL, one-way ANOVA with post-hoc Tukey HSD test. (J–L) WISH results of *lcp1*⁺ leukocytes in CHT of 48 hpf zebrafish embryos. **, $p < 0.01$ compared with CTRL, one-way ANOVA with post-hoc Tukey HSD test. (M–O) WISH results of *hbae1.1*⁺ erythrocytes in the CHT of 48 hpf zebrafish embryos. No significant difference was found between CTRL and *atg* mutations, chi-squared test. All the CHT results in WISH pictures were straightened using ImageJ.

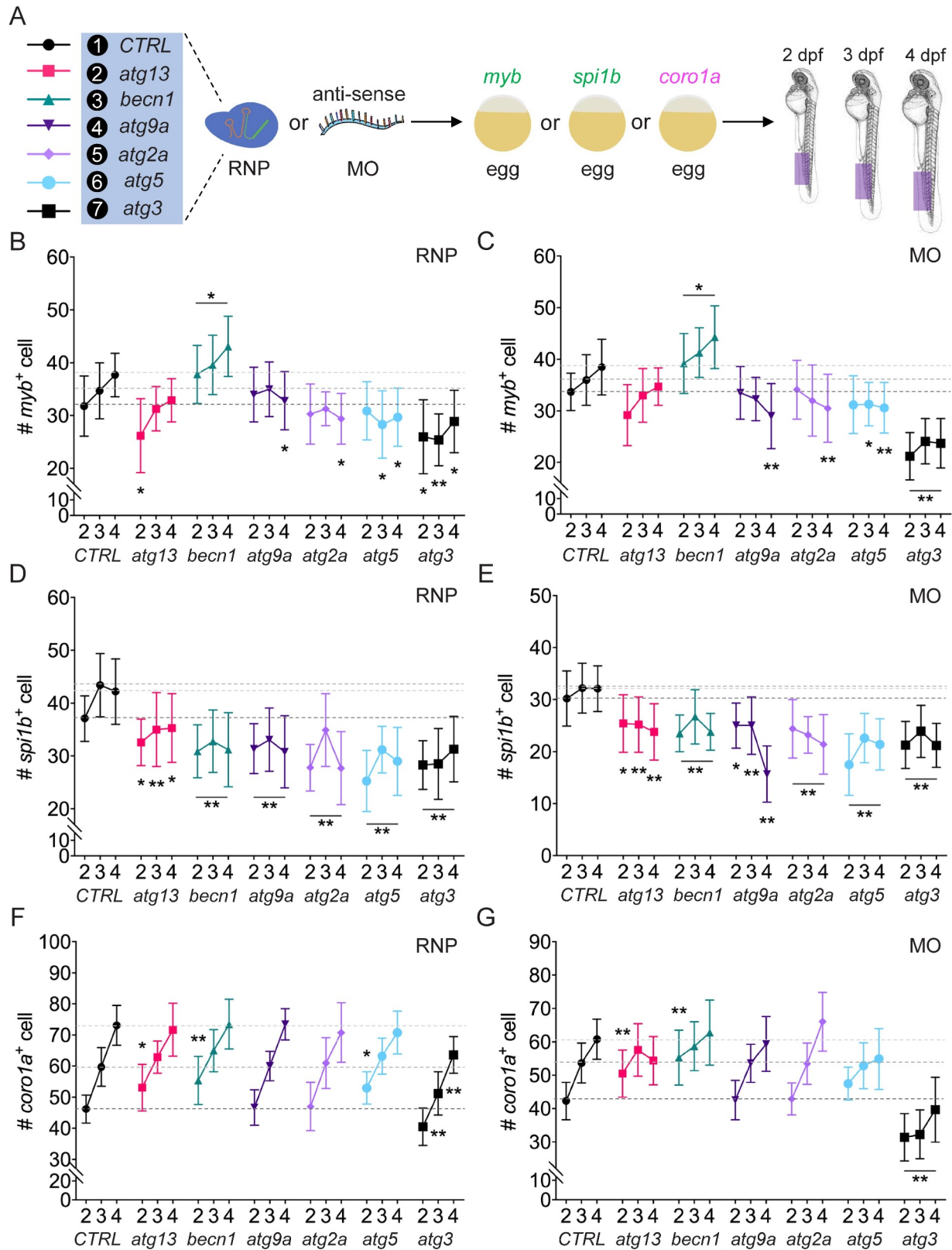


Figure 5. Time-dependent effects of core *atg* mutations on zebrafish definitive hematopoiesis. (A) experimental setup for the time-dependent effect of CRISPR-Cas9 RNP- or MO-based *atg* mutations on definitive hematopoiesis from 2 to 4 dpf. (B-D) effects of CRISPR-Cas9 RNP-based *atg* mutations on *myb*⁺ HSPCs, *spi1b*⁺ myeloid progenitor cells, and *coro1a*⁺ leukocytes from 2 to 4 dpf. *, $p < 0.05$, **, $p < 0.01$ compared with CTRL, one-way ANOVA with post-hoc Tukey HSD test. (E-G) effects of MO-based *atg* mutations on *myb*⁺ HSPCs, *spi1b*⁺ myeloid progenitor cells, and *coro1a*⁺ leukocytes from 2 to 4 dpf. *, $p < 0.05$, **, $p < 0.01$ compared with CTRL, one-way ANOVA with post-hoc Tukey HSD test.

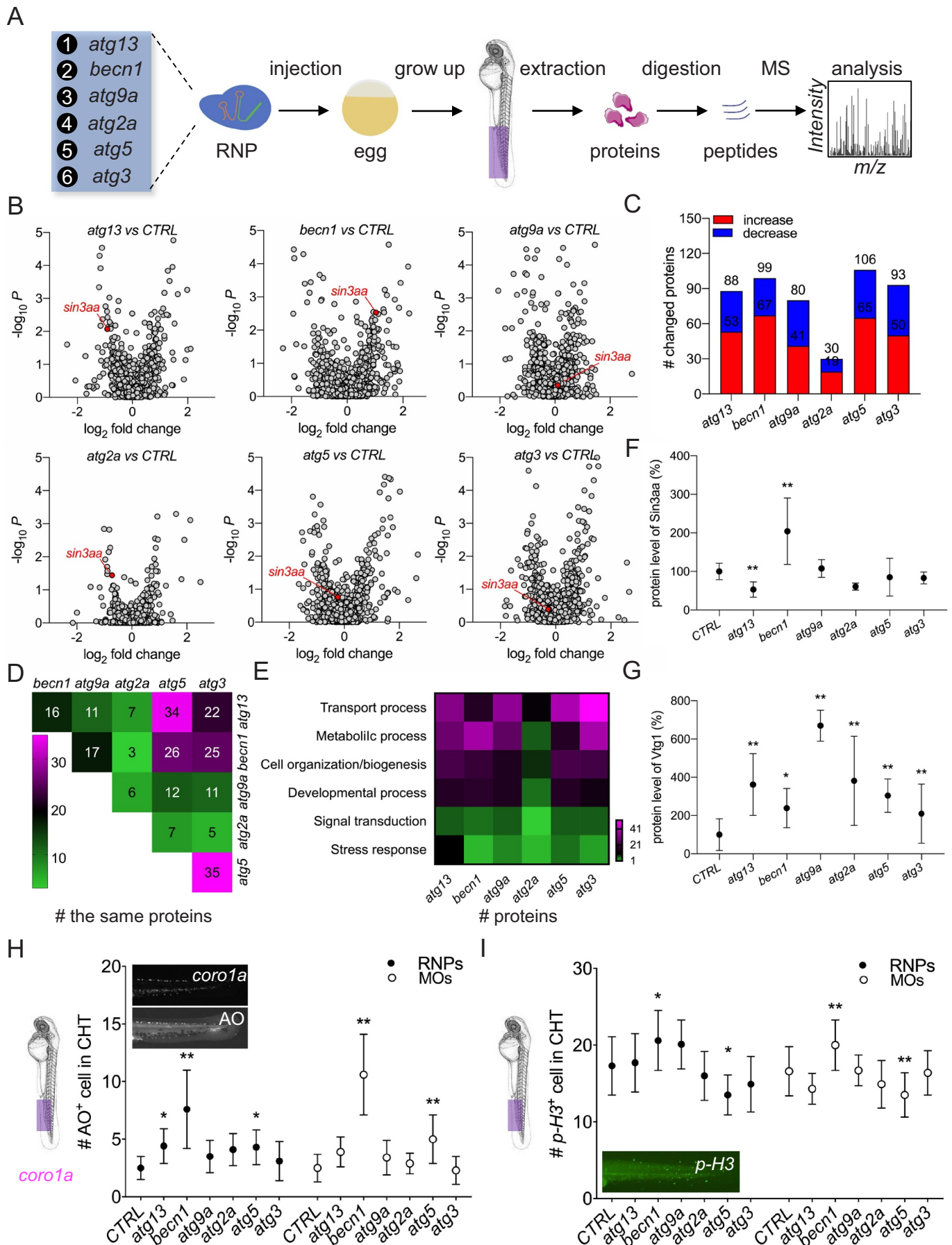


Figure 6. Mass spectrometry-based proteomic and cellular variabilities among *atg* mutations. (A) experimental setup for mass spectrometry-based proteomic analysis of the CHT region of zebrafish embryos with various *atg* mutations. (B) volcano map of *atg* mutations comparing with CTRL. Red dot, Sin3aa (SIN3 transcription regulator family member a) protein. (C-D) comparison of the number (#) of significantly changed proteins, including both increased and decreased proteins, and the

lethality in accordance with a previous report [24]. This suggests the consistency of the role of *atg/Atg* genes in the early development between zebrafish and mice [3]. As core *ATG* genes that primarily facilitate the formation of autophagosome in autophagy process, the level of autophagosomes in response to *atg13*, *becn1*, and *atg5* knockout (KO) or KD has been previously studied in zebrafish, whereas studies on *atg9a*, *atg2a*, and *atg3* mutations are not yet reported. Of these, MO-based KD of *atg13* and *atg5* decreased the level of autophagosomes, characterized by declined levels of Lc3-II protein and *Lc3*⁺ puncta in zebrafish [25,26]. In the present study, similar reductions in autophagosome numbers were also observed after CRISPR-Cas9 RNP or MO-based *atg13* or *atg5* targeting. Conversely, contradictory results were observed in *becn1* mutations, in which MO-based KD of exon two or four of *becn1* targeting in this and previous studies attenuated the level of autophagosomes, while exon seven of *becn1* targeting increased the level of autophagosomes in another study [26–28]. These results suggested a mutation type-dependent effect of *becn1* mutation on autophagosome formation, and targeting early exons of *becn1* may be required for the inhibition of autophagosome formation. More importantly, to our knowledge, this is the first study that described the functions of *atg9a*, *atg2a*, and *atg3* mutations in the autophagy of zebrafish embryos. Since *ATG9A* and *ATG3* are responsible for autophagosome formation and LC3 lipidation, respectively [29,30], a decreased level of autophagosome was observed in zebrafish embryos with *atg9a* and *atg3* mutations. In addition, disruption of *ATG2A* is associated with impaired autophagic flux and accumulation of immature autophagosomal membranes in mammalian cells [31], which was reproduced in *atg2a*-mutant zebrafish embryos. By using CQ treatment and *Tg(GFP-Lc3:RFP-Lc3ΔG)* zebrafish line, we also found *atg13* and *atg3* mutations affected the autophagic flux in zebrafish embryos, probably through distinct mechanisms by inhibiting the autophagosome formation or LC3 lipidation [30,32]. Altogether, the function of various *atg* genes in the canonical autophagy process conservatively between zebrafish and mammals, and CRISPR-Cas9 RNP targeting resulted in a similar loss of function as homozygous mutation and MO-based KD in zebrafish embryos.

Despite the autophagy deficiency in zebrafish embryos with various *atg* mutations, our work showed that the hematopoietic abnormalities varied between *atg* mutations. Of these, *becn1*, *atg13*, and *atg3* mutations showed considerable but different effects on zebrafish definitive hematopoiesis. This observation implied that regulator effects of various core *atg* genes are, at least partially, canonical autophagy-independent as observed in previous mice studies [9–13]. However, little is known about the specific core *Atg* genes-dependent hematopoietic effects in mice since none of previous studies included comparisons among several *Atg* genes, and very few core *Atg*

genes have been studied in mice. The present study determined that *becn1* mutation induced HSPCs expansion and transiently increased leukocytes and neutrophils in zebrafish during embryonic development. Although the up-regulator effects of *becn1* KD on HSPCs have been reported in zebrafish embryos with *KRI1 homolog* mutation [33], our work for the first time identified the sole role of *becn1* mutation in HSPCs expansion during normal hematopoiesis, which can be ascribed to the altered regulator proteins of HSPCs [34] or disturbances among autophagy, apoptosis, and differentiation [35]. The ortholog of *Sin3a*, an epigenetic modifier essential to HSCs maintenance and hematopoiesis in mice [36], was found to be up-regulated following *becn1* mutation. Further co-mutation results also confirmed that *becn1* mutation-based HSPCs regulation is *sin3aa*-dependent. Conversely, the level of HSPCs, including long term-HSC and HSC-containing lineage⁻/*Spinocerebellar ataxia type 1*⁺/*KIT proto-oncogene, receptor tyrosine kinase*⁺ (LSK) cells, elevated in the spleen while they declined in bone marrow in adult mice with *becn1* CKO in hematopoietic cells [12]. Thus, *Becn1/becn1* behaves heterogeneously in the regulation of HSPCs between zebrafish and mice. It could be explained by that mouse HSCs reside in both spleen and bone marrow, whereas the HSPCs largely resided in the CHT of zebrafish larvae. Besides, this discrepancy could also be attributed to the unaltered autophagy and autophagic flux in HSPCs of mice with *becn1* CKO [12]. Strikingly, myeloid cell-specific *becn1* CKO increased the neutrophil and leukocytes but not the macrophages in mice, which was consistent with our findings in zebrafish embryos [37]. Also, a similar expansion of hematopoietic lineages was reported in a fruit fly (*Drosophila melanogaster*) model with *atg6/becn1* KO [38]. These findings indicated that the expansion of neutrophils and leukocytes in zebrafish with *becn1* mutation may be due to the loss of *becn1* in myeloid progenitor cells without affecting the HSCs since HSCs minimally contribute to zebrafish definitive hematopoiesis in the early stage [39].

Conversely, *atg13* mutation showed the opposite effect to *becn1* mutation in HSPCs, in which it lowered the level of HSPCs in zebrafish embryos in a *sin3aa*-dependent manner. Although no study has explored the roles of *atg13* mutation in definitive hematopoiesis, our findings provide preliminary but important evidence that core *atg* genes could play opposite roles in definitive hematopoiesis by modulating the same regulator. In addition, *atg3* mutation showed down-regulator effects on HSPCs, myeloid progenitor cells, and leukocytes, including both neutrophils and macrophages in zebrafish embryos, which is in accordance with hematopoietic defects observed in *atg7* CKO mice probably due to the involvement of both *Atg7* and *Atg3* in *Lc3-PE* conjugation system [10]. However, evidence on hematopoietic responses to *ATG3* mutation in mammals has not yet been reported. Unlike

number of consistent proteins among *atg* mutations. (E) biological process enrichment of significantly altered proteins in various *atg* mutants. (F-G) protein levels of *Sin3aa* and *Vtg1* (Vitellogenin 1) among *atg* mutations. **, $p < 0.01$ compared with CTRL, analyzed by progenesis Q1 software. (H) the number of apoptotic *coro1a*⁺ leukocytes in the CHT was measured by using acridine orange (AO) live staining. *, $p < 0.05$, **, $p < 0.01$ compared with CTRL, one-way ANOVA with post-hoc Tukey HSD test. (H) the number of cells undergoing mitosis in the CHT measured by using *p-H3* (phospho-histone H3) immunostaining. *, $p < 0.05$, **, $p < 0.01$ compared with CTRL, one-way ANOVA with post-hoc Tukey HSD test.

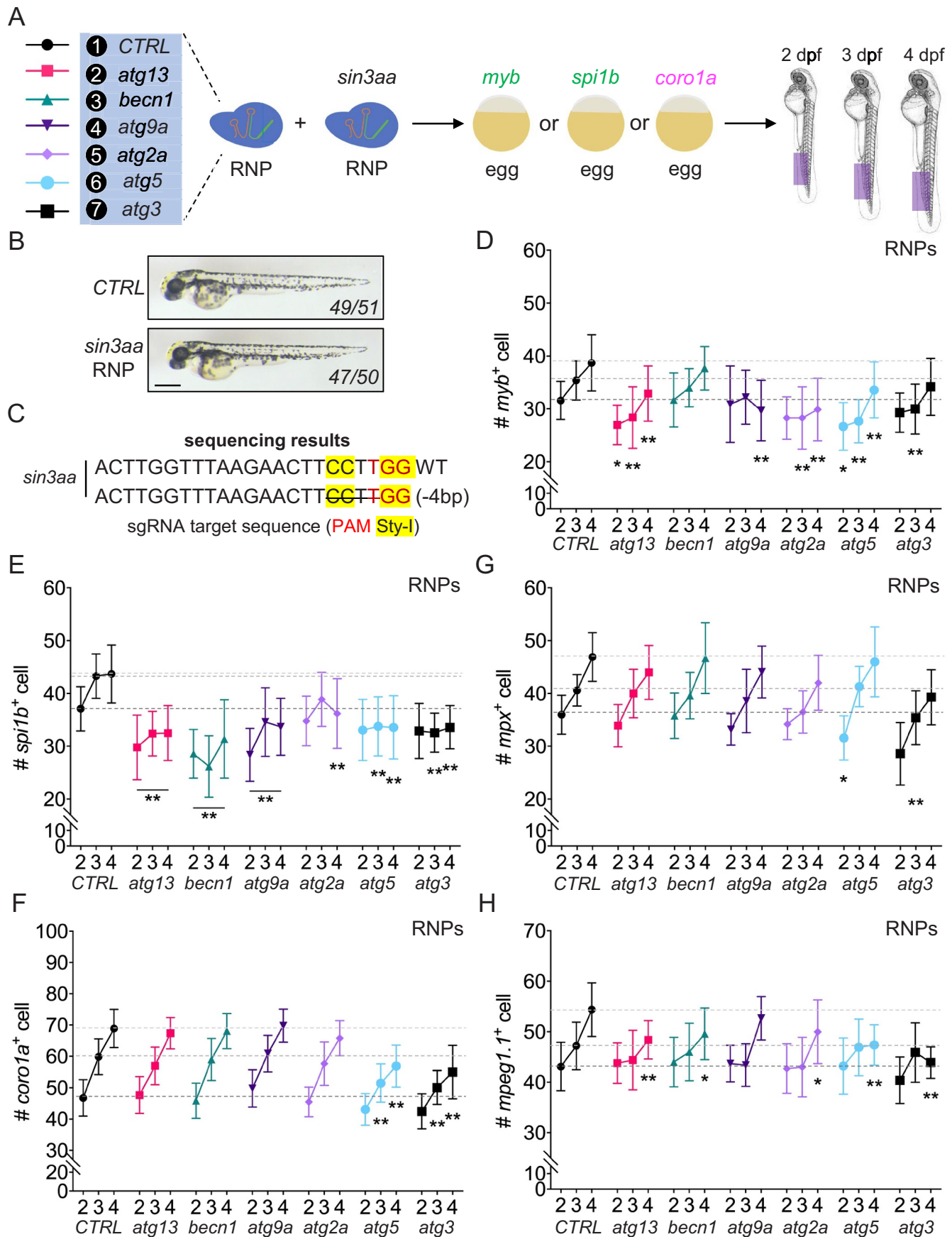


Figure 7. *sin3aa* contributes to HSPCs regulation by *becn1* and *atg13* in zebrafish embryos. (A) experimental setup for the time-dependent hematopoietic responses to co-mutation of *sin3aa* with various *atg* genes. (B-C) representative morphology of 2 dpf zebrafish embryos with *sin3aa* mutation and sequencing results of the representative mutation. Scale bar: 0.5 mm. (D-H) time-dependent effects of co-mutation of *sin3aa* with various *atg* genes on *myb*⁺ HSPCs, *spi1b*⁺ myeloid progenitor cells, *coro1a*⁺ leukocytes, *mpx*⁺ neutrophils, and *mpeg1.1*⁺ macrophages from 2 to 4 dpf. *, $p < 0.05$, **, $p < 0.01$ compared with CTRL, one-way ANOVA with post-hoc Tukey HSD test.

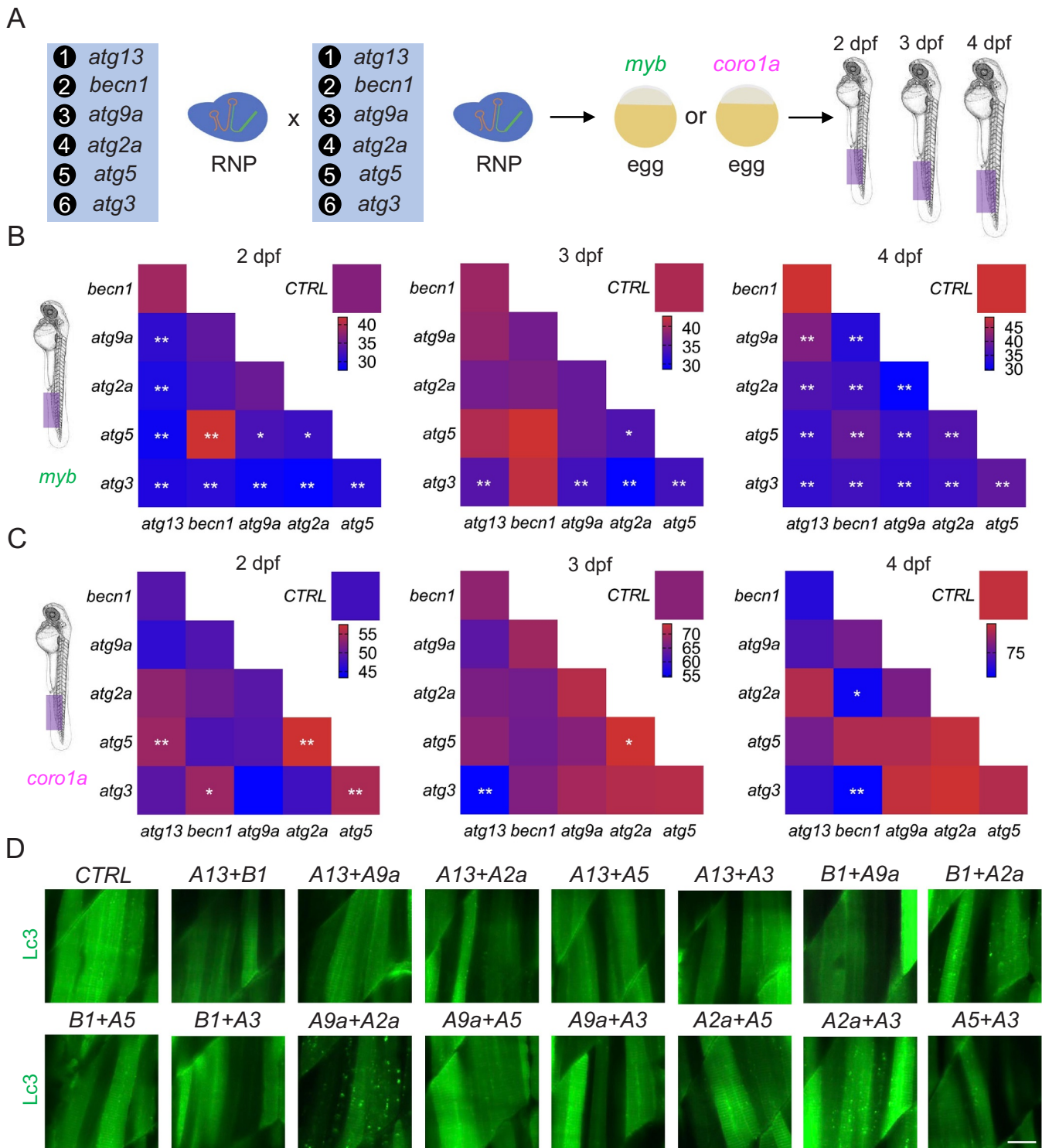


Figure 8. Time-dependent effects of core *atg* genes double mutations on zebrafish definitive hematopoiesis. (A) experimental setup for the time-dependent responses of *myb*⁺ HSPCs and *coro1a*⁺ leukocytes to double mutations of every two *atg* genes. (B) time-dependent effect of core *atg* double mutations on *myb*⁺ HSPCs during the period from 2 to 4 dpf. *, $p < 0.05$, **, $p < 0.01$ compared with CTRL, one-way ANOVA with post-hoc Tukey HSD test. (C) time-dependent effect of core *atg* double mutations on *coro1a*⁺ leukocytes during the period from 2 to 4 dpf. *, $p < 0.05$, **, $p < 0.01$ compared with CTRL, one-way ANOVA with post-hoc Tukey HSD test. (D) effect of core *atg* double mutations on *Lc3*⁺ puncta in 2 dpf zebrafish embryos. A, *atg*; B, *becn1*. Scale bar: 50 μ m.

becn1 and *atg13*, the level of *sin3aa* remained unchanged in *atg3* mutant zebrafish embryos, suggesting the existence of another mechanisms underlying core *atg* gene-regulated

definitive hematopoiesis in zebrafish, which required further investigations. In summary, mutation of *ATG* genes that belong to the same autophagy machinery may share the

feature of hematopoietic abnormalities and core *ATG* genes could play different even opposite roles in vertebrate definitive hematopoiesis.

In addition to the distinct effects of various core *atg* genes on HSPCs, leukocytes, neutrophils, and macrophages, myeloid progenitor cells showed similar responses to all the *atg* mutations, which may be regulated through the canonical autophagy pathway. We also identified *vtg1*, an estrogen responder that was up-regulated in all the *atg* mutations, suggesting a potential alteration in estrogen under *atg* mutations. A previous study has revealed that estrogen impaired the HSPCs production by interfering with the hemogenic endothelial niche [40]. Thus, the consistent responses of myeloid progenitor cells in zebrafish with various *atg* mutations may be due to the interactions between canonical autophagy-regulated estrogen and the niche of hematopoietic cells in zebrafish embryos, though further studies are needed. Conversely, the responses of myeloid progenitor cells in mice differed between *Atg* genes CKO [9–13], which is potentially due to developmental stage differences [14]. More importantly, we also confirmed the interplays between core *atg* genes. Hematopoietic defects in *atg3* mutants are largely independent of other core *atg* genes, whereas HSPCs expansion in *becn1* mutant zebrafish embryos largely depends on the presence of other core *atg* genes. It suggests that *atg3* itself may be essential to definitive hematopoiesis, while *becn1*-independent non-canonical autophagy likely contributes to HSPCs expansion. Our findings further highlight the need to study multiple *ATG* genes and their interplays simultaneously. However, only one study on definitive hematopoiesis was documented in mice with double *atg* gene KOs, which revealed an indispensable *Ulk1*-mediated *Atg5*-independent autophagy in the regulation of erythropoiesis [41]. The interactions between other *ATG* genes in other lineage hematopoiesis remain concealed. Zebrafish provide an alternative platform to study non-canonical autophagy and non-autophagy functions of various core *ATG* genes *in vivo*. Despite our work providing a more comprehensive picture of various core *ATG* genes in the regulation of vertebrate definitive hematopoiesis than previous studies, the limitations of this study cannot be neglected: 1) the effects of *atg* mutations are limited to zebrafish definitive hematopoiesis in the embryonic stage; 2) cell-autonomous and non-cell-autonomous effects of *atg* genes cannot be distinguished, and 3) more *ATG* genes and their combinations are needed, which ultimately calls for the use of inducible hematopoietic cell-specific multiplex *atg* genes KO and more advanced proteomic analysis in future studies.

Materials and methods

Zebrafish strains and husbandry

Transgenic and wild-type zebrafish were maintained in 14:10 h light:dark cycle and fed brine shrimp twice daily. *Tg(GFP-Lc3)* [42], *Tg(myb:GFP)* (zf289Tg), *Tg(coro1a:DsRed)* [43], *Tg(spi1b:GFP)* (zdf11Tg), *Tg(mpx:mCherry)* [44], *Tg(mpeg1.1:Dendra2)* [45], and *Tg(GFP-Lc3:RFP-Lc3ΔG)* [46] zebrafish lines were used in this study. Zebrafish embryos were raised

at 28.5°C and staged by dpf and morphological criteria as previously described [47]. All animal experiments were performed in accordance with protocols approved by Animal Subjects Ethics Sub-Committee (ASESC) of The Hong Kong Polytechnic University.

CRISPR-Cas9 ribonucleoprotein and morpholino targeting

Target sites and sgRNA of zebrafish *atg* genes (*atg13*, *becn1*, *atg9a*, *atg2a*, *atg5*, and *atg3*) or *sin3aa* were identified and designed using Alt-R® CRISPR-Cas9 guide RNA design tool (Integrated DNA Technologies) or CRISPRscan [48]. Target sites were chosen that the one with 1) good on-target score, 2) acceptable off-target score, and 3) a restriction enzyme site around the protospacer adjacent motif (PAM) sequence. Target sequence and restriction enzyme site of *atg* genes-targeting sgRNA used in this study were listed in Figure 1C and Figure S1E. Given the target sequences of sgRNA, CRISPR-Cas9 RNPs were generated and delivered to zebrafish embryos as previously described [20]. Briefly, synthetic Alt-R® CRISPR-Cas9 sgRNA (Integrated DNA Technologies) was folded at 95°C for 5 min and then cooled down to the room temperature. Alt-R® S.p. Cas9 Nuclease V3 (Integrated DNA Technologies 1,081,059) diluted in Cas9 working buffer (20 mM HEPES, 150 mM KCl, pH 7.5) and subsequently was assembled with folded sgRNA in 37°C for 10 min. Around 2 nl CRISPR-Cas9 RNP was delivered into the cell of zebrafish embryos at the one-cell stage through microinjection. For co-injection, two CRISPR-Cas9 RNPs were formed individually and then mixed before micro-injection. Around 4 nl CRISPR-Cas9 RNPs were injected into the cell of zebrafish embryos. Almost no toxic effect of these CRISPR-Cas9 RNPs was observed in zebrafish embryos after microinjection. On the other hand, MOs targeting *atg13*, *becn1*, and *atg5* were pre-designed [26,49,50], while *atg9a*, *atg2a*, and *atg3* were designed by Gene Tools, LLC (Figure 1F). All MOs were purchased from Gene Tools, LLC and confirmed by using *Tg(GFP-LC3)* zebrafish line as previously described [25]. Diluted *atg* genes-targeting MO was micro-injected into zebrafish embryos at the one-cell stage and standard control MO was injected as CTRL [51].

Restriction fragment length polymorphism assay

Mutagenesis and mutagenic efficiency were detected by using RFLP assay as previously described [19]. Briefly, a 300 to 600 bp PCR fragment covering the designed sgRNA target site was amplified for each *atg* gene using corresponding primers listed in Table S1. Next, the restriction enzyme (listed in Figure S1E, New England Biolabs) was then used to cleave the PCR fragment, in which the uncleaved band suggested a destroyed restriction enzyme site by CRISPR-Cas9 RNP-induced mutations, while the cleaved band contained original sequence. Mutagenic efficiency was calculated by dividing the intensity of the uncleaved band by the intensity of the total band measured by ImageJ (NIH). To further confirm the mutations, uncleaved band was sub-cloned into pGEM®-T Easy

Vector (Promega Corporation, A1360) and the insertions and deletions (indels) were identified by Sanger sequencing.

Fluorescence-activated cell sorting and Cyto-ID staining

Single-cell suspension for FACS was prepared as described previously [52]. Briefly, *Tg(coro1a:DsRed)* zebrafish embryos at 3 dpf were digested with Gibco™ Trypsin-EDTA (0.05%) (Thermo Fisher 25,300,062) for 15 min at 28°C and then disassociated with pipetting on ice. After termination of Trypsin with CaCl₂ (2 mM), the suspension was filtered using a 40-µm cell strainer (BD Biosciences 352,340) and washed with phosphate-buffered saline (PBS) (VWR Life Science, E404-200TABS) with 1% (vol:vol) fetal bovine serum (Thermo Fisher 26,140,079). FACS of *coro1a:DsRed*⁺ leukocyte was then conducted in BD FACSAria III Cell Sorter according to the manufacturer's instructions. Around 8,000 *coro1a:DsRed*⁺ cells were targeted to be sorted using a “purity sort” mode. Autophagic vacuoles and nucleus in sorted cells were immediately stained using CYTO-ID® Autophagy detection kit 2.0 with Hoechst 33,342 Nuclear Stain (Enzo Life Sciences, ENZ-KIT175) at 37°C in dark following the manufacturer's instructions [21]. CYTO-ID® Autophagy Dye and Hoechst 33,342 co-stained leukocytes were washed with 1X assay buffer before fluorescence microscopic imaging.

Fluorescence microscope imaging

Fluorescent images of transgenic zebrafish embryos, stained zebrafish embryos, or sorted *coro1a*⁺ cells stained with CYTO-ID® Autophagy Dye and Hoechst 33,342 were taken by using Zeiss Lightsheet Z.1 Selective Plane Illumination Microscope, Leica TCS SPE Confocal Microscope, or Nikon Stereomicroscope with a Nikon DS-Fi2 Camera as previously described [42]. Zebrafish embryos were mounted in 1.5% low-melting agarose (Sigma-Aldrich, A9045) into a 35-mm glass-bottom confocal dish or glass capillary before imaging. Tricaine (Sigma-Aldrich, A5040) at 0.16 mg/ml in E3 medium (5 mM NaCl, 0.17 mM KCl, 0.33 mM CaCl₂, and 0.33 mM MgSO₄, pH 7.4) was used as an anesthetic for zebrafish embryos. In addition, *Tg(GFP-Lc3)* zebrafish embryo was treated with CQ (Selleckchem, S4157) at 100 µM in E3 medium before imaging.

Whole-mount in situ hybridization

WISH was performed on zebrafish embryos following the standard protocol described previously [52]. DIG-labeled anti-sense probes (*myb*, *spilb*, *lcp1*, *hbae1.1*, and *rag1*) were made from the pGEM®-T Easy vector (Promega Corporation, A1360) containing the gene-coding sequences via *in vitro* transcription using DIG RNA Labeling Kit (Roche 11,175,025,910). Bleaching in a short period of time was used to remove the pigments from the fixed zebrafish embryos.

Mass spectrometry-based proteomics

Total protein was extracted from the CHT region of zebrafish embryos using cell lysis buffer (Sigma-Aldrich, C3228) as previously described [53]. Purified protein was then digested into peptides using Trypsin (Promega, V5111) and desalted using Pierce C18 Spin Columns (Thermo Fisher 89,870). A label-free quantitative proteomics was conducted on Thermo Fisher Orbitrap Fusion Lumos Mass Spectrometer coupled with Dionex UltiMate 3000 RSLCnano. Identification and quantification were processed with Progenesis QI software, and the abundance of proteins was quantified based on three independent experiments and normalized based on total protein. Arbitrary fold change cutoffs of > 1.5 and significance *p*-values of 0.05 were set for significantly up-regulated or down-regulated proteins.

Acridine orange and phospho-histone H3 staining

Live *Tg(coro1a:DsRed)* zebrafish embryos at 2 dpf were incubated with AO (Sigma-Aldrich, A6014) at 10 µg/ml in dark for 30 min and washed with fish water before fluorescence imaging. Whole-mount immunostaining of cells undergoing mitosis was conducted in fixed zebrafish embryos using *p-H3* primary antibody (Cell Signaling Technology, 9701) following the manufacturer's protocol [51].

Quantification and statistics

The number of *Lc3*⁺ puncta in the muscle was counted in Zeiss ZEN software following the criteria and protocol described in our previous study [42]. Cyto-ID⁺ autophagic vacuoles were defined by vacuole-like GFP⁺ fluorescence signals that were distinguished from the background and a similar size of autophagic vacuoles was considered in all the autophagic vacuoles counting in the cells. In addition, ImageJ (NIH) was utilized to measure the relative intensity of proteins in western blot and straighten the WISH images. Data are reported as mean ± standard deviation (S.D.). One-way analysis of variance (ANOVA) with post-hoc Tukey HSD Test, Chi-squared test, and independent t-test were performed where appropriate using Statistical Package for the Social Sciences (SPSS) Version 14.0, and a *p*-value less than 0.05 was considered statistically significant.

Acknowledgements

The zebrafish maintenance was supported by the Fish Model Translational Research Laboratory (HTI, PolyU). Light-sheet or confocal fluorescence microscopic imaging, flow cytometry, and mass spectrometry-based proteomics were supported by the University Research Facility in Life Sciences (ULS, PolyU).

Disclosure statement

No potential conflict of interest was reported by the author(s).

Funding

The work was supported by the Health and Medical Research Fund [03143765]; Health and Medical Research Fund [06173226]; The Hong Kong Polytechnic University Postdoc Matching Fund Scheme Research Grants Council, University Grants Committee [T12-702/20-N].

Data availability statement

MS data are available upon request.

ORCID

Xiang-Ke Chen  <http://orcid.org/0000-0003-2069-6634>

Zhen-Ni Yi  <http://orcid.org/0000-0003-4876-4248>

Alvin Chun-Hang Ma  <http://orcid.org/0000-0002-4800-2844>

References

- Jiang P, Mizushima N. Autophagy and human diseases. *Cell Res.* 2014;24(1):69–79. doi: [10.1038/cr.2013.161](https://doi.org/10.1038/cr.2013.161)
- Suzuki H, Osawa T, Fujioka Y, et al. Structural biology of the core autophagy machinery. *Curr Opin Struct Biol.* 2017;43:10–17. doi: [10.1016/j.sbi.2016.09.010](https://doi.org/10.1016/j.sbi.2016.09.010)
- Kuma A, Komatsu M, Mizushima N. Autophagy-monitoring and autophagy-deficient mice. *Autophagy.* 2017;13(10):1619–1628. doi: [10.1080/15548627.2017.1343770](https://doi.org/10.1080/15548627.2017.1343770)
- Collier JJ, Guissart C, Oláhová M, et al. Developmental consequences of defective ATG7-mediated autophagy in humans. *N Engl J Med.* 2021;384(25):2406–2417. doi: [10.1056/NEJMoa1915722](https://doi.org/10.1056/NEJMoa1915722)
- Nishida Y, Arakawa S, Fujitani K, et al. Discovery of Atg5/Atg7-independent alternative macroautophagy. *Nature.* 2009;461(7264):654–658. doi: [10.1038/nature08455](https://doi.org/10.1038/nature08455)
- Codogno P, Mehrpour M, Proikas-Cezanne T. Canonical and non-canonical autophagy: variations on a common theme of self-eating? *Nat Rev Mol Cell Biol.* 2011;13(1):7–12. doi: [10.1038/nrm3249](https://doi.org/10.1038/nrm3249)
- Galluzzi L, Green DR. Autophagy-independent functions of the autophagy machinery. *Cell.* 2019;177(7):1682–1699. doi: [10.1016/j.cell.2019.05.026](https://doi.org/10.1016/j.cell.2019.05.026)
- Sawyers CL, Denny CT, Witte ON. Leukemia and the disruption of normal hematopoiesis. *Cell.* 1991;64(2):337–350. doi: [10.1016/0092-8674\(91\)90643-D](https://doi.org/10.1016/0092-8674(91)90643-D)
- Jung HE, Shim YR, Oh JE, et al. The autophagy protein Atg5 plays a crucial role in the maintenance and reconstitution ability of hematopoietic stem cells. *Immune Netw.* 2019;19(2):e12. doi: [10.4110/in.2019.19.e12](https://doi.org/10.4110/in.2019.19.e12)
- Mortensen M, Soilleux EJ, Djordjevic G, et al. The autophagy protein Atg7 is essential for hematopoietic stem cell maintenance. *J Exp Med.* 2011;208(3):455–467. doi: [10.1084/jem.20101145](https://doi.org/10.1084/jem.20101145)
- Liu F, Lee JY, Wei H, et al. FIP200 is required for the cell-autonomous maintenance of fetal hematopoietic stem cells. *Blood.* 2010;116(23):4806–4814. doi: [10.1182/blood-2010-06-288589](https://doi.org/10.1182/blood-2010-06-288589)
- Yang X, Ge L, Wang J. BECN1 modulates hematopoietic stem cells by targeting caspase-3-GSDME-mediated pyroptosis. *Blood Sci.* 2020;2(3):89–99. doi: [10.1097/BS9.0000000000000051](https://doi.org/10.1097/BS9.0000000000000051)
- Ho TT, Warr MR, Adelman ER, et al. Autophagy maintains the metabolism and function of young and old stem cells. *Nature.* 2017;543(7644):205–210. doi: [10.1038/nature21388](https://doi.org/10.1038/nature21388)
- Hashimoto M, Umemoto T, Nakamura-Ishizu A, et al. Autophagy is dispensable for the maintenance of hematopoietic stem cells in neonates. *Blood Adv.* 2021;5(6):1594–1604. doi: [10.1182/bloodadvances.2020002410](https://doi.org/10.1182/bloodadvances.2020002410)
- Davidson AJ, Zon LI. The ‘definitive’ (and ‘primitive’) guide to zebrafish hematopoiesis. *Oncogene.* 2004;23(43):7233–7246. doi: [10.1038/sj.onc.1207943](https://doi.org/10.1038/sj.onc.1207943)
- He C, Bartholomew CR, Zhou W, et al. Assaying autophagic activity in transgenic GFP-Lc3 and GFP-Gabarap zebrafish embryos. *Autophagy.* 2009;5(4):520–526. doi: [10.4161/auto.5.4.7768](https://doi.org/10.4161/auto.5.4.7768)
- Howe K, Clark MD, Torroja CF, et al. The zebrafish reference genome sequence and its relationship to the human genome. *Nature.* 2013;496(7446):498–503. doi: [10.1038/nature12111](https://doi.org/10.1038/nature12111)
- Bill BR, Petzold AM, Clark KJ, et al. A primer for morpholino use in zebrafish. *Zebrafish.* 2009;6(1):69–77. doi: [10.1089/zeb.2008.0555](https://doi.org/10.1089/zeb.2008.0555)
- Bedell VM, Wang Y, Campbell JM, et al. In vivo genome editing using a high-efficiency TALEN system. *Nature.* 2012;491(7422):114–118. doi: [10.1038/nature11537](https://doi.org/10.1038/nature11537)
- Hoshijima K, Jurynek MJ, Klatt Shaw D, et al. Highly efficient CRISPR-Cas9-based methods for generating deletion mutations and F0 embryos that lack gene function in zebrafish. *Dev Cell.* 2019;51(5):645–657.e4. doi: [10.1016/j.devcel.2019.10.004](https://doi.org/10.1016/j.devcel.2019.10.004)
- Guo S, Liang Y, Murphy SF, et al. A rapid and high content assay that measures cyto-ID-stained autophagic compartments and estimates autophagy flux with potential clinical applications. *Autophagy.* 2015;11(3):560–572. doi: [10.1080/15548627.2015.1017181](https://doi.org/10.1080/15548627.2015.1017181)
- Huang G, Zhang F, Ye Q, et al. The circadian clock regulates autophagy directly through the nuclear hormone receptor Nr1d1/Rev-erba and indirectly via Cebpb/(C/ebpβ) in zebrafish. *Autophagy.* 2016;12(8):1292–1309. doi: [10.1080/15548627.2016.1183843](https://doi.org/10.1080/15548627.2016.1183843)
- Mortensen M, Watson AS, Simon AK. Lack of autophagy in the hematopoietic system leads to loss of hematopoietic stem cell function and dysregulated myeloid proliferation. *Autophagy.* 2011;7(9):1069–1070. doi: [10.4161/auto.7.9.15886](https://doi.org/10.4161/auto.7.9.15886)
- Morishita H, Kanda Y, Kaizuka T, et al. Autophagy is required for maturation of surfactant-containing lamellar bodies in the lung and swim bladder. *Cell Rep.* 2020;33(10):108477. doi: [10.1016/j.celrep.2020.108477](https://doi.org/10.1016/j.celrep.2020.108477)
- Masud S, Prajsnar TK, Torraca V, et al. Macrophages target salmonella by Lc3-associated phagocytosis in a systemic infection model. *Autophagy.* 2019;15(5):796–812. doi: [10.1080/15548627.2019.1569297](https://doi.org/10.1080/15548627.2019.1569297)
- Lee E, Koo Y, Ng A, et al. Autophagy is essential for cardiac morphogenesis during vertebrate development. *Autophagy.* 2014;10(4):572–587. doi: [10.4161/auto.27649](https://doi.org/10.4161/auto.27649)
- Mawed SA, Zhang J, Ren F, et al. atg7 and beclin1 are essential for energy metabolism and survival during the larval-to-juvenile transition stage of zebrafish. *Aquac Fish.* 2021;7(4):359–372. doi: [10.1016/j.aaf.2021.01.002](https://doi.org/10.1016/j.aaf.2021.01.002)
- Dong G, Zhang Z, Duan K, et al. Beclin 1 deficiency causes hepatic cell apoptosis via endoplasmic reticulum stress in zebrafish larvae. *FEBS Lett.* 2020;594(7):1155–1165. doi: [10.1002/1873-3468.13712](https://doi.org/10.1002/1873-3468.13712)
- Imai K, Hao F, Fujita N, et al. Atg9A trafficking through the recycling endosomes is required for autophagosome formation. *J Cell Sci.* 2016;129:3781–3791. doi: [10.1242/jcs.196196](https://doi.org/10.1242/jcs.196196)
- Nath S, Dancourt J, Shteyn V, et al. Lipidation of the LC3/GABARAP family of autophagy proteins relies on a membrane-curvature-sensing domain in Atg3. *Nat Cell Biol.* 2014;16(5):415–424. doi: [10.1038/ncb2940](https://doi.org/10.1038/ncb2940)
- Tang Z, Takahashi Y, Chen C, et al. Atg2A/B deficiency switches cytoprotective autophagy to non-canonical caspase-8 activation and apoptosis. *Cell Death Differ.* 2017;24(12):2127–2138. doi: [10.1038/cdd.2017.133](https://doi.org/10.1038/cdd.2017.133)
- Puente C, Hendrickson RC, Jiang X. Nutrient-regulated phosphorylation of ATG13 inhibits starvation-induced autophagy. *J Biol Chem.* 2016;291(11):6026–6035. doi: [10.1074/jbc.M115.689646](https://doi.org/10.1074/jbc.M115.689646)

- [33] Jia X-E, Ma K, Xu T, et al. Mutation of krill causes definitive hematopoiesis failure via PERK-dependent excessive autophagy induction. *Cell Res.* 2015;25(8):946–962. doi: [10.1038/cr.2015.81](https://doi.org/10.1038/cr.2015.81)
- [34] Huang HT, Kathrein KL, Barton A, et al. A network of epigenetic regulators guides developmental haematopoiesis in vivo. *Nat Cell Biol.* 2013;15(12):1516–1525. doi: [10.1038/ncb2870](https://doi.org/10.1038/ncb2870)
- [35] Wang J. Beclin 1 bridges autophagy, apoptosis and differentiation. *Autophagy.* 2008;4(7):947–948. doi: [10.4161/auto.6787](https://doi.org/10.4161/auto.6787)
- [36] Heideman MR, Lancini C, Proost N, et al. Sin3a-associated Hdac1 and Hdac2 are essential for hematopoietic stem cell homeostasis and contribute differentially to hematopoiesis. *Haematologica.* 2014;99(8):1292–1303. doi: [10.3324/haematol.2013.092643](https://doi.org/10.3324/haematol.2013.092643)
- [37] Tan P, He L, Xing C, et al. Myeloid loss of Beclin 1 promotes PD-L1hi precursor B cell lymphoma development. *J Clin Invest.* 2019;129(12):5261–5277. doi: [10.1172/JCI127721](https://doi.org/10.1172/JCI127721)
- [38] Shrivage BV, Hill JH, Powers CM, et al. Atg6 is required for multiple vesicle trafficking pathways and hematopoiesis in drosophila. *Development.* 2013;140(6):1321–1329. doi: [10.1242/dev.089490](https://doi.org/10.1242/dev.089490)
- [39] Ulloa BA, Habbsa SS, Potts KS, et al. Definitive hematopoietic stem cells minimally contribute to embryonic hematopoiesis. *Cell Rep.* 2021;36(11):109703. doi: [10.1016/j.celrep.2021.109703](https://doi.org/10.1016/j.celrep.2021.109703)
- [40] Carroll KJ, Esain V, Garnaas MK, et al. Estrogen defines the dorsal-ventral limit of VEGF regulation to specify the location of the hemogenic endothelial niche. *Dev Cell.* 2014;29(4):437–453. doi: [10.1016/j.devcel.2014.04.012](https://doi.org/10.1016/j.devcel.2014.04.012)
- [41] Honda S, Arakawa S, Nishida Y, et al. Ulk1-mediated Atg5-independent macroautophagy mediates elimination of mitochondria from embryonic reticulocytes. *Nat Commun.* 2014;5(1):4004. doi: [10.1038/ncomms5004](https://doi.org/10.1038/ncomms5004)
- [42] Chen XK, Kwan JS, Chang RC, et al. 1-phenyl 2-thiourea (PTU) activates autophagy in zebrafish embryos. *Autophagy.* 2020;17(5):1222–1231. 2020/04/15. doi: [10.1080/15548627.2020.1755119](https://doi.org/10.1080/15548627.2020.1755119)
- [43] Yan B, Han P, Pan L, et al. Il-1 β and reactive oxygen species differentially regulate neutrophil directional migration and basal random motility in a zebrafish injury-induced inflammation model. *J Immunol.* 2014;192(12):5998–6008. 2014/05/20. doi: [10.4049/jimmunol.1301645](https://doi.org/10.4049/jimmunol.1301645)
- [44] Yoo SK, Deng Q, Cavnar PJ, et al. Differential regulation of protrusion and polarity by PI(3)K during neutrophil motility in live zebrafish. *Dev Cell.* 2010;18(2):226–236. doi: [10.1016/j.devcel.2009.11.015](https://doi.org/10.1016/j.devcel.2009.11.015)
- [45] Harvie EA, Green JM, Neely MN, et al. Innate immune response to streptococcus iniae infection in zebrafish larvae. *Infect Immun.* 2013;81(1):110–121. doi: [10.1128/IAI.00642-12](https://doi.org/10.1128/IAI.00642-12)
- [46] Kaizuka T, Morishita H, Hama Y, et al. An autophagic flux probe that releases an internal control. *Mol Cell.* 2016;64(4):835–849. doi: [10.1016/j.molcel.2016.09.037](https://doi.org/10.1016/j.molcel.2016.09.037)
- [47] Kimmel CB, Ballard WW, Kimmel SR, et al. Stages of embryonic development of the zebrafish. *Dev Dyn.* 1995;203(3):253–310. 1995/07/01. doi: [10.1002/aja.1002030302](https://doi.org/10.1002/aja.1002030302)
- [48] Moreno-Mateos MA, Vejnar CE, Beaudoin JD, et al. Crisprscan: designing highly efficient sgRNAs for CRISPR-Cas9 targeting in vivo. *Nat Methods.* 2015;12(10):982–988. doi: [10.1038/nmeth.3543](https://doi.org/10.1038/nmeth.3543)
- [49] Musso G, Tasan M, Mosimann C, et al. Novel cardiovascular gene functions revealed via systematic phenotype prediction in zebrafish. *Development.* 2014;141(1):224–235. doi: [10.1242/dev.099796](https://doi.org/10.1242/dev.099796)
- [50] Hu Z, Zhang J, Zhang Q. Expression pattern and functions of autophagy-related gene atg5 in zebrafish organogenesis. *Autophagy.* 2011;7(12):1514–1527. doi: [10.4161/auto.7.12.18040](https://doi.org/10.4161/auto.7.12.18040)
- [51] Chen XK, Kwan JK, Wong GC, et al. Leukocyte invasion of the brain after peripheral trauma in zebrafish (*Danio rerio*). *Exp Mol Med.* 2022;54(7):973–987. doi: [10.1038/s12276-022-00801-4](https://doi.org/10.1038/s12276-022-00801-4)
- [52] Ma AC, Ward AC, Liang R, et al. The role of jak2a in zebrafish hematopoiesis. *Blood.* 2007;110(6):1824–1830. 2007/06/05. doi: [10.1182/blood-2007-03-078287](https://doi.org/10.1182/blood-2007-03-078287)
- [53] Xia J, Kang Z, Xue Y, et al. A single-cell resolution developmental atlas of hematopoietic stem and progenitor cell expansion in zebrafish. *Proc Natl Acad Sci U S A.* 2021;118(14):118. doi: [10.1073/pnas.2015748118](https://doi.org/10.1073/pnas.2015748118)